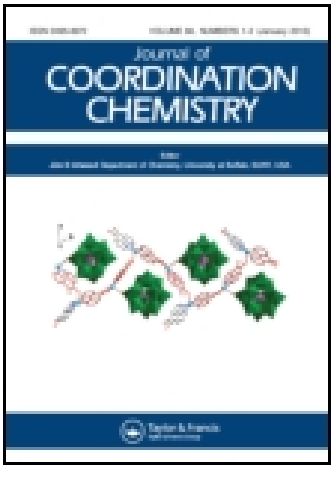

Journal of Coordination Chemistry
Publication details, including instructions for authors and subscription information:
http://www.tandfonline.com/loi/gcoo20

Synthesis, characterization, thermal behavior, and DFT aspects of some oxovanadium(IV) complexes involving ONO-donor sugar Schiff bases

R.C. Maurya[a], B.A. Malik[a], J.M. Mir[a] & A.K. Sharma[a]
[a] Coordination and Bioinorganic Chemistry Laboratory, Department of P.G. Studies and Research in Chemistry and Pharmacy, R.D. University, Jabalpur, India
Accepted author version posted online: 01 Sep 2014.Published online: 25 Sep 2014.

To cite this article: R.C. Maurya, B.A. Malik, J.M. Mir & A.K. Sharma (2014) Synthesis, characterization, thermal behavior, and DFT aspects of some oxovanadium(IV) complexes involving ONO-donor sugar Schiff bases, Journal of Coordination Chemistry, 67:18, 3084-3106, DOI: 10.1080/00958972.2014.959508

To link to this article: http://dx.doi.org/10.1080/00958972.2014.959508

Journal of Coordination Chemistry, 2014
Vol. 67, No. 18, 3084–3106, http://dx.doi.org/10.1080/00958972.2014.959508

Synthesis, characterization, thermal behavior, and DFT aspects of some oxovanadium(IV) complexes involving ONO-donor sugar Schiff bases

R.C. MAURYA*, B.A. MALIK, J.M. MIR and A.K. SHARMA

Coordination and Bioinorganic Chemistry Laboratory, Department of P.G. Studies and Research in Chemistry and Pharmacy, R.D. University, Jabalpur, India

(*Received 24 April 2014; accepted 29 July 2014*)

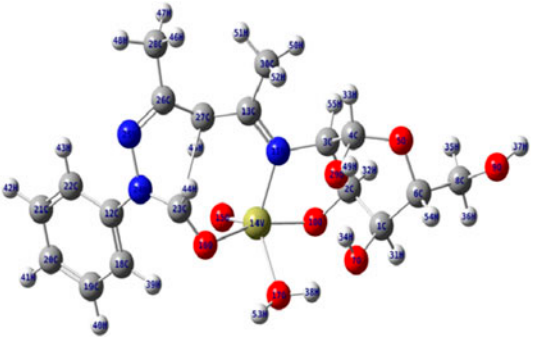

Optimized structure of Complex [VO(ampph-gls)(H_2O)]

Seven new Schiff base complexes of oxovanadium(IV) of the general composition [VO(L)(H_2O)], where **H_2L** = H_2bmpph-gls, H_2bumpph-gls, H_2*iso*-vmpph-gls, H_2pmpph-gls, H_2*iso*-bumpph-gls, H_2ampph-gls, and H_2vmpph-gls has been synthesized by the reaction of **$VOSO_4 \cdot 5H_2O$** and the said ligands in aqueous ethanol medium.

Seven new Schiff base complexes of oxovanadium(IV), [VO(L)(H_2O)], where **H_2L** = H_2bmpph-gls, H_2bumpph-gls, H_2*iso*-vmpph-gls, H_2pmpph-gls, H_2*iso*-bumpph-gls, H_2ampph-gls, and H_2vmpph-gls, have been synthesized by the reaction of **$VOSO_4 \cdot 5H_2O$** and the said ligands in aqueous ethanol. The resulting complexes have been characterized on the basis of elemental analysis, vanadium determination, molar conductance, magnetic measurements, thermogravimetric (TG) analysis, infrared, electronic mass, and electron spin resonance studies. The thermal decomposition processes of one representative complex is discussed, and the order of reaction (n) and the activation energies (E_a) have been calculated from TG and differential TG curves. Molecular geometry optimizations, molecular surface electrostatic potentials, vibrational frequency calculations, bond lengths, bond angles and dihedral angles, and natural atomic charges obtained by natural bond orbital and Mulliken population analysis and calculations of molecular energies, highest occupied molecular orbital and lowest unoccupied molecular orbital were performed with the Gaussian 09 software package using density functional theory methods with Becke3–Lee–Yang–Parr (B3LYP) hybrid exchange–correlation functional and the standard 6-311G(+) basis set for (ampph-glsH_2) and LANL2DZ basis set for one of

*Corresponding author. Email: rcmaurya1@gmail.com

its complexes, [VO(ampph-gls)(H_2O)]. No imaginary frequency was found in the optimized model compounds, and hence it ensures that the molecule is in the lowest point of the potential energy surface, that is, an energy minimum. Finally calculated results were applied to simulate infrared spectra which show good agreement with observed spectra. Based on experimental and theoretical data, suitable square pyramidal structures have been proposed for these complexes.

Keywords: Oxovanadium(IV) complexes; ONO-donor amino sugar-based organic matrix; Bioinorganic; Medicinal relevance; 3-D Molecular modeling

1. Introduction

The ability of sugars to sequester metals is of current interest in the possible development of metal chelates for clinical use and as models for biologically important compounds [1–6]. Amino sugars form Schiff base with salicylaldehyde and other aromatic aldehydes, and only few reports of transition metal complexes of these ligands have been found [7]. Metal chelation could be a rational therapeutic approach for interdicting Alzheimer's disease (AD) pathogenesis. Amyloid plaques are clusters of proteins and metal ions accumulated between neurons (nerve cells) in Alzheimer's patients' brains. Enhancing the targeting and efficacy of metal ion-chelating agents through sugar-appended ligand is a recent strategy in the development of the next generation of metal chelators [8].

Vanadium is a trace but essential element with relevant biological properties and has acquired special status among the biometals. Vanadium (IV and V) ions experience extensive redox chemistry under physiological (pH 3–7) conditions [9–11]. Structural and/or functional models for these enzymes, vanadate-dependent haloperoxidases and vanadium nitrogenase, have also stimulated the coordination chemistry of vanadium [12]. Interest has emerged in vanadium chemistry pertaining to its catalytic [13], antiparasitic [14], and antihyperglycemic properties [15–19]. Vanadium Schiff base complexes due to various structural models reported so far have received great attention. Four idealized geometries have been explored in oxovanadium(IV) complexes, retaining the short V–O bond, octahedral [20–22], square pyramidal [23], trigonal prismatic [24], or trigonal bipyramidal. The last configuration is usually found only in protein complexes [25].

Pyrazolines are attractive drug scaffolding compounds with many biological applications [26, 27] and have been reported to possess strong antibacterial, antihistaminic, and antifungal activities [28, 29]. Their derivatives are present in a number of pharmacologically active molecules. Changes in their structure have offered a high degree of diversity useful for the development of new therapeutic agents having improved potency and less toxicity [30, 31].

There are only a few publications on vanadium complexes with ligands containing sugars [32], particularly the preparation of compounds in the solid state [33–38]. Sugars or amino sugars have gained much interest for acting as non-toxic ligating compounds. D-Glucosamine is known to promote the formation and repair of cartilage, and it has been used in dietary supplements as a remedy for the treatment of osteoarthritis [39–41]. Vanadium along with other metals has been designated as tau marker in cerebrospinal fluid in patients with AD [42, 43] and has also been reported as a chelating therapeutic agent for the treatment of AD [44]. Its Schiff base complexes have pronounced DNA binding [45]. Oxovanadium–sugar complexes are often too soluble or not stable enough for complexes to be prepared. Introducing an anchoring group into a sugar molecule enhances its coordinating behavior by several orders of magnitude [32]. Schiff base

compounds obtained by the reaction of 4-acyl-3-methyl-1-phenyl-2-pyrazolin-5-one and α,D-glucosamine may be highly interesting compounds in this respect.

Thermal analysis techniques are extensively used in studying thermal behavior of metal complexes [46–49]. Density functional theory (DFT) is a powerful method for predicting the geometry of vanadium compounds [50, 51, 53, 54]. It is useful for investigation of large molecules as well [55]. The Cartesian representations of theoretical force constants are usually computed at optimized geometry by assuming Cs point group symmetry. To show the existence of intramolecular charge transfer (ICT) within molecular system, energies of the highest occupied molecular orbital (HOMO) and lowest unoccupied molecular orbital (LUMO) levels and the molecular electrostatic surface potential (MESP) energy surface studies are manipulated by DFT [56].

In view of the importance of vanadium compounds, ability of sugars to sequester metals and various utilities of computational DFT studies, herein, we report the synthesis of some amino sugar–Schiff base ligands (obtained by interaction of different acyl derivatives of 3-methyl-1phenyl-2-pyrazoline-5-one and glucosamine hydrochloride) (figure 1), along with their oxovanadium(IV) complexes.

2. Experimental

2.1. *Materials*

Vanadyl sulfate pentahydrate, 3-methyl-1-phenyl-2-pyrazoline-5-one (Lancaster, UK), D-glucosamine hydrochloride (Lancaster, UK), benzoyl chloride, acetyl chloride, propionyl chloride, butyryl chloride (Thomas Baker Chemicals Limited, Mumbai), *iso*-butyryl chloride (Merck), valeryl chloride, and *iso*-valeryl chloride (Lancaster, UK) were used as supplied. All other chemicals used were of analytical grade.

2.2. *Preparation of ligands*

A solution of glucosamine hydrochloride (0.01 M) in 20 mL methanol–water (50%) is treated with 10 mL aqueous solution of sodium carbonate (0.01 M, 0.84 g), filtered if necessary. To the filtrate the respective 4-acyl-3-methyl-1-phenyl-2-pyrazolin-5-one (0.01 M) was

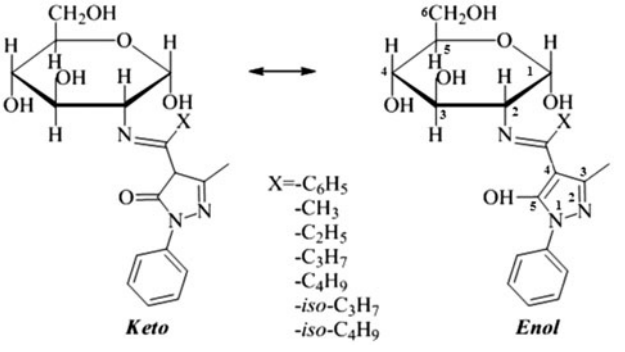

Figure 1. Keto and enol forms of Schiff bases.

added and dissolved in 20 mL methanol. The resulting solution is refluxed with stirring for 4 h at 20–30 °C. The solution was kept cool overnight. The precipitate so obtained is filtered with suction, washed several times with water and finally with methanol–water (50%) and dried *in vacuo*.

2.3. *Preparation of complexes*

The vanadyl complexes were prepared by the addition of ethanolic solution of the ligands (0.01 M, 10 mL) to a warm solution of **$VOSO_4 \cdot 5H_2O$** (0.01M, 2.53 g) in ethanol (50%, 15 mL). The resulting solution was refluxed with stirring for 4 h. The desired complex was filtered with suction, washed several times with 1 : 1 ethanol–water solution and dried *in vacuo*.

2.4. *Analysis*

Carbon, hydrogen, and nitrogen were determined microanalytically at SAIF, Indian Institute of Technology, Mumbai. The vanadium content of each of the complexes was determined as follows. A 100 mg of the sample of the compound was placed in a silica crucible, decomposed by gentle heating and then 1–2 mL of concentrated $HNO_3$was added 2–3 times. An orangish mass (V_2O_5) was obtained after decomposing and complete drying. It was dissolved in the minimum amount of dilute H_2SO_4, and the solution so obtained was diluted with distilled water to 100 mL in a measuring flask. The vanadium content of each of the complexes was determined volumetrically using decinormal $KMnO_4$ solution as an oxidizing agent in the presence of sulfurous acid. The amount of vanadium in the sample solution was calculated using the standard [57] relationship: 1 mL of 0.1 N $KMnO_4$ = 5.094 mg vanadium.

3. Physical methods

The following physical methods were used to determine the structure of the ligand and their resulting oxovanadium (IV) complexes. Solid-state IR spectra were recorded in KBr pellets using PerkinElmer model 1620 FT-IR Spectrophotometer at IIT, Roorkee. Electronic spectra were recorded using ATI Unicam UV-2-100 UV/Visible Spectrophotometer in our laboratory; EPR Spectra of the complexes were recorded at LNT at RSIC, IIT, Chennai. Thermogravimetric (TG) analyses of the complexes were performed on a Perkin-Elmer (Pyris Diamond) Thermoanalyzer at Institute Instrumentation Center, IIT, Roorkee. The C, H, and N were determined at RSIC, IIT, Bombay.

4. Computational methods

In order to understand the vibrational properties and structural characteristics of the ligands and complexes, the DFT calculation [58] with B3LYP/6-311+G and B3LYP/LANL2DZ combinations have been used, respectively, and the observed bands are assigned based on the results of normal coordinate analysis. The assignment of the calculated wave numbers

was aided by the animation option of Gauss View 5.0 graphical interface for Gaussian programs, which gives a visual presentation of the shape of the vibrational modes [59, 60]. The Cartesian representations of the theoretical force constants are usually computed at optimized geometry by assuming Cs point group symmetry. The energies of the HOMO and LUMO levels and the MESP energy surface studies were used for determining the existence of ICT [56].

To obtain a deeper understanding of the interaction between vanadium metal ion and O_4 environment, *ab initio* total energy calculations within the DFT framework were carried out for H_2ampph-gls and one of the representative synthesized complexes. The optimized structures, vibrational frequencies, HOMO–LUMO, Mulliken charges, and natural bond orbital (NBO) charges are presented and discussed. All the theoretical calculations manifested by Gaussian 09 software package were performed at the Department of P.G. Studies and Research in Chemistry and Pharmacy, RD University, Jabalpur, MP, India.

5. Results and discussion

The formation of the Schiff bases is consistent with the microanalytical data. The melting points, colors, and yields are given in table 1, while the microanalytical data and important infrared spectral bands of the ligands are given in table 2. The formation of the Schiff bases is confirmed by the appearance of the azomethine peak at 1603–1633 cm^{-1} in infrared spectra of all the ligands.

The oxovanadium(IV) complexes were prepared as per the reaction given below:

$$\mathbf{VOSO_4 \cdot 5H_2O} + H_2L \xrightarrow[\text{Reflux}]{\text{Ethanol, } H_2O} [VO(L)(H_2O)] + \mathbf{4H_2O} + H_2SO_4$$

where $\mathbf{H_2L}$ = H_2bmpph-gls, H_2bummpph-gls, H_2*iso*-vmpph-gls, H_2pmpph-gls, H_2*iso*-bumpph-gls, H_2ampph-gls, and H_2vmpph-gls.

These complexes are air-stable, thermally stable, and their decomposition temperatures are given in table 3. These are insoluble in most common organic solvents, but are fairly soluble in DMF, DMSO, and acetonitrile. The formulation of these complexes is based on their physicochemical and theoretical studies.

5.1. *Infrared spectral studies*

The important infrared spectral bands and their tentative assignments for the synthesized ligands and complexes are given in tables 2 and 4, respectively. All the complexes exhibit a

Table 1. Some physical properties of synthesized ligands.

Ligand	Empirical formula	MW	Color	Decomposition temp. (°C)
H_2bmpph-gls	$C_{23}H_{25}N_3O_6$	439	Middle buff	160
H_2bumpph-gls	$C_{20}H_{27}N_3O_6$	405	Golden brown	160
H_2*iso*-vmpph-gls	$C_{21}H_{29}N_3O_6$	419	Sandstone	140
H_2pmpph-gls	$C_{19}H_{25}N_3O_6$	391	Middle buff	155
H_2*iso*-bumpph-gls	$C_{20}H_{27}N_3O_6$	405	Middle buff	140
H_2ampph-gls	$C_{18}H_{23}N_3O_6$	377	Golden brown	155
H_2vmpph-gls	$C_{21}H_{29}N_3O_6$	419	Canary yellow	158

Table 2. Analytical data and important IR spectral bands (cm^{-1}) and their assignments.

Ligand (Empirical formula) (MW)	Analysis, Found (Calcd %)			ν(C=N) (azomethine)	ν(–OH)	ν(C–O) (enolic)	ν(C=N) (pyrazolone skeleton)
	C	H	N				
H_2bmpph-gls ($C_{23}H_{25}N_3O_6$) (439)	62.98 (62.87)	5.43 (5.69)	9.43 (9.57)	1611	3480	1140	1597
H_2bumpph-gls ($C_{20}H_{27}N_3O_6$) (405)	59.49 (59.26)	6.75 (6.67)	10.13 (10.37)	1624	3585	1173(w)	1591
H_2*iso*-vmpph-gls ($C_{21}H_{29}N_3O_6$) (419)	60.41 (60.14)	6.62 (6.92)	10.55 (10.02)	1630	3490	1175	1570
H_2pmpph-gls ($C_{19}H_{25}N_3O_6$) (391)	58.18 (58.31)	6.61 (6.39)	10.42 (10.74)	1603	3400	1150	1572
H_2*iso*-bumpph-gls ($C_{20}H_{27}N_3O_6$) (405)	59.61 (59.26)	6.45 (6.67)	10.82 (10.37)	1633	3500	1172	1590
H_2ampph-gls ($C_{18}H_{23}N_3O_6$) (377)	57.52 (57.29)	6.20 (6.10)	11.56 (11.14)	1621	3480	1172	1589
H_2vmpph-gls ($C_{21}H_{29}N_3O_6$) (419)	60.52 (60.14)	6.40 (6.92)	10.45 (10.02)	1628	3410	1150	1590

strong band at 893–977 cm^{-1} which has been assigned to ν(V=O) [61], suggesting that interaction of a V=O unit with another V=O unit is not possible, indicating the absence of a –V=O…V=O– chain structure [62–64] in the present complexes. The Schiff bases used in the present investigation may exist in the keto (I) and enol (II) forms (figure 1). However, the appearance of a weak broad band at 3400–3500 cm^{-1} in all the ligands suggests that they exist in enol form in the solid state. Hence, H_2bmpph-gls, H_2bumpph-gls, H_2*iso*-vmpph-gls, H_2pmpph-gls, H_2*iso*-bumpph-gls, H_2ampph-gls, and H_2vmpph-gls contain four potential donor sites: (i) the ring nitrogen N^1, (ii) the ring nitrogen N^2, (iii) the enolic oxygen (–OH), and (iv) the azomethine nitrogen. Moreover, the hydroxyl groups of the glucosamine attached to C_1 and C_3 in the neighborhood of azomethine nitrogen may also coordinate with the metal center. However, considering the planarity of the ligands, it is unlikely that they could act as a hexadentate ligand towards a single metal. Hence, these ligands seemed to be potentially tridentate through (i) enolic oxygen (–OH), (ii) azomethine nitrogen, and (iii) C_3 hydroxyl oxygen (glucosamine moiety). The coordination of the ring nitrogen N^1 is ruled out because of the presence of a bulky phenyl group attached to it. The coordination of the ring nitrogen N^2 is also ruled out because it lies opposite to the enolic oxygen in the pyrazolone skeleton. The same argument may also be given to the non-participation of C_1-hydroxyl oxygen of the glucosamine part as it is also present at the opposite side of the azomethine nitrogen.

The ligands under discussion show a sharp and strong band due to ν(C=N) of the azomethine group at 1603–1633 cm^{-1}. The observed low energy shift of this band in the range 1594–1620 cm^{-1} in the complexes suggests the coordination of the azomethine nitrogen [65]. The infrared spectra of all the Schiff bases show a medium band at 1140–1175 cm^{-1} assigned to ν(C–O) (enolic). In the spectra of the corresponding complexes, this band shifts to higher wavenumber at 1163–1220 cm^{-1}, suggesting coordination of the enolic oxygen after deprotonation. The appearance of a broad band centered at 3450–3500 cm^{-1} suggests the presence of coordinated water in these complexes.

Introduction of an anchoring group into a sugar molecule, which as a primary coordinating site may promote the deprotonation/coordination of the alcoholic hydroxyl groups, the complex forming ability of the sugar derivative may be enhanced several orders of

Table 3. Analytical data and some physical properties of the synthesized complexes.

Complex (Empirical formula) Molecular weight	Found/calculated (%)				Color	Decomp. Temp. (°C)	Λ_M ($\Omega^{-1}cm^2M^{-1}$)	μ_{eff} (BM)	Yield (%)
	C	H	N	V					
[VO(bmpph-gls)(H_2O)]	52.56	4.95	8.22	9.58	Pale cream	275	25	1.70	48
($C_{23}H_{25}N_3O_7V$) (521.94)	(52.87)	(4.78)	(8.04)	(9.76)					
[VO(bumpph-gls)(H_2O)]	49.40	5.45	8.28	10.65	Middle buff	205	20	1.68	45
($C_{20}H_{27}N_3O_7V$) (487.94)	(49.18)	(5.53)	(8.60)	(10.44)					
[VO(*iso*-vmpph-gls)(H_2O)]	50.56	5.41	8.03	10.57	Raw silk	250	36	1.71	42
($C_{21}H_{29}N_3O_7V$) (501.94)	(50.20)	(5.77)	(8.36)	(10.14)					
[VO(pmpph-gls)(H_2O)]	48.42	5.49	8.53	10.94	Sand stone	280	42	1.69	44
($C_{19}H_{25}N_3O_7V$) (473.94)	(48.10)	(5.27)	(8.86)	(10.74)					
[VO(*iso*-bumpph-gls)(H_2O)]	49.53	5.37	8.28	10.71	Middle buff	150	48	1.70	43
($C_{20}H_{27}N_3O_7V$) (487.94)	(49.18)	(5.53)	(8.60)	(10.44)					
[VO(ampph-gls)(H_2O)]	46.49	5.13	9.31	11.26	Canary yellow	315	41	1.71	46
($C_{18}H_{23}N_3O_7V$) (459.94)	(46.96)	(5.00)	(9.13)	(11.07)					
[VO(vmpph-gls)(H_2O)]	50.01	5.98	8.72	10.46	Pistachio	>320	34	1.71	38
($C_{21}H_{29}N_3O_7V$) (501.94)	(50.20)	(5.77)	(8.36)	(10.14)					

Table 4. Some important IR spectral bands (cm^{-1}) of the synthesized complexes.

Complex	*ν*(V=O)	*ν*(C=N)	*ν*(C–O)	*ν*(V–O)	*ν*(V–N)	(OH)
[VO(bmpph-gls)(H_2O)]	900	1601	1163	470	420	3450
[VO(bumpph-gls)(H_2O)]	893	1612	1173	450 (sharp)	437	3490
[VO(*iso*-vmpph-gls)(H_2O)]	903	1605	1200	456	430	3500
[VO(pmpph-gls)(H_2O)]	899	1594	1180	476	407	3500
[VO(*iso*-bumpph-gls)(H_2O)]	970	1620	1173 (sharp)	488	450	3500
[VO(ampph-gls)(H_2O)]	974	1611	1220	460	420	3500
[VO(vmpph-gls)(H_2O)]	977	1607	1170	470	450	3480

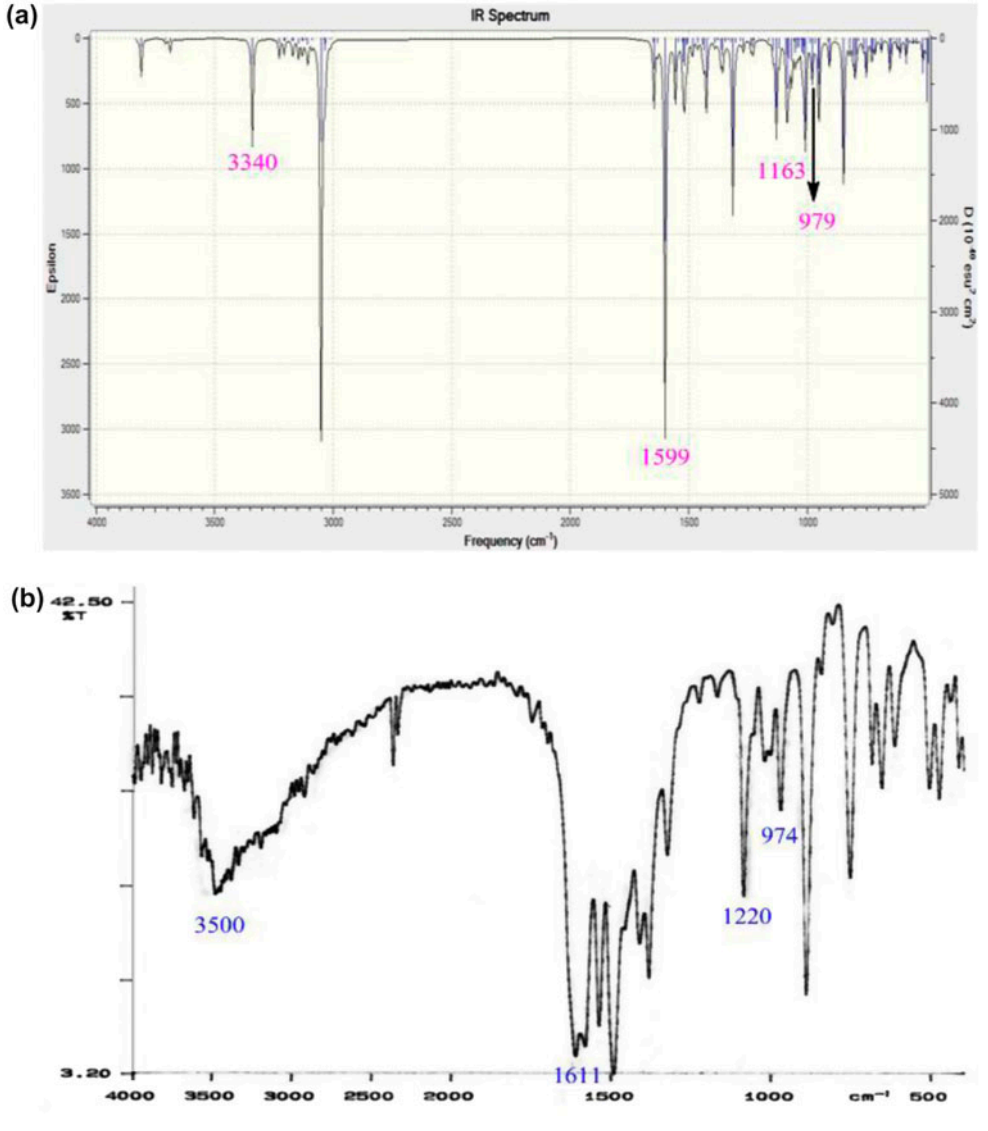

Figure 2. IR spectrum of [VO(ampph-gls)(H_2O)] (a) theoretical and (b) experimental.

magnitude [66]. Schiff base ligands obtained by the reaction of D-glucosamine and 4-acyl-3-methyl-1-phenyl-2-pyrazolin-5-one in the present investigation may be interesting ligands in this respect. In view of the above discussion and considering the analytical data supporting 1 : 1 metal–ligand ratio, plus the square pyramidal geometry as evidenced by the electronic spectral data (*vide infra*), it seems logical that the C_3-alcoholic hydroxyl group of the present ligands is coordinating to the metal center after deprotonation besides the azomethine nitrogen and enolic oxygen as the donor sites. The molar conductance data with respect to the non-electrolytic nature of the complex are also consistent with dibasic tridentate (*ONO*) nature of the present ligands. The infrared spectral data failed to explain the coordination of the deprotonated C_3-alcoholic hydroxyl group in all these complexes due to the presence of a broad band at ~3500 cm^{-1} on account of three more free alcoholic hydroxyl groups and also due to the presence of a coordinated water molecule in all the complexes.

The DFT computational IR spectrum of one of the representative compounds [VO(ampph-gls)(H_2O)] shows close resemblance with the important spectral bands with that of corresponding experimental spectral bands as shown in figure 2.

5.2. *Conductance measurements*

The observed molar conductances (20–48 Ω^{-1} $cm^2 M^{-1}$) in 10^{-3} molar DMF solutions of these complexes, given in table 3, are consistent with the non-electrolytic nature of the complexes. Such a non-zero molar conductance value for each of the complex in the present study is most probably due to the strong donor capacity of DMF, which may lead to the displacement of anionic ligand and change of electrolyte [67] type.

5.3. *Magnetic measurements*

The oxovanadium(IV) is a $S = 1/2$ system. The magnetically dilute oxovanadium(IV) complexes usually exhibit magnetic moments to their spin-only value of 1.73 BM. At room temperature, the observed value of the magnetic moments for the present complexes is in

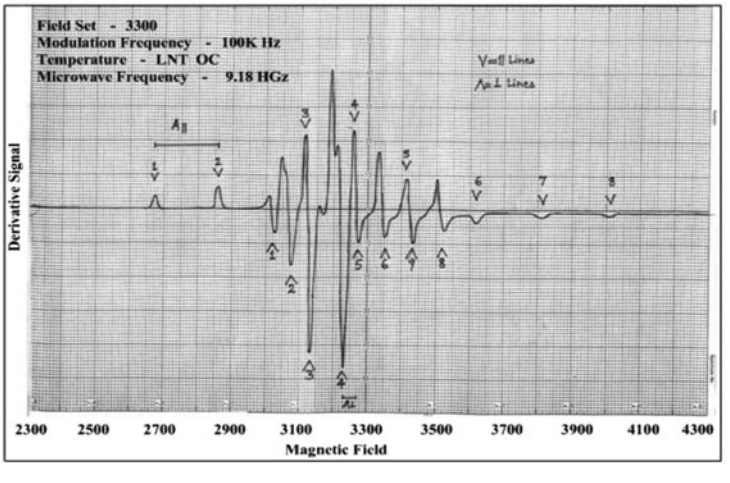

Figure 3. ESR spectrum of [VO(bmpph-gls)(H_2O)].

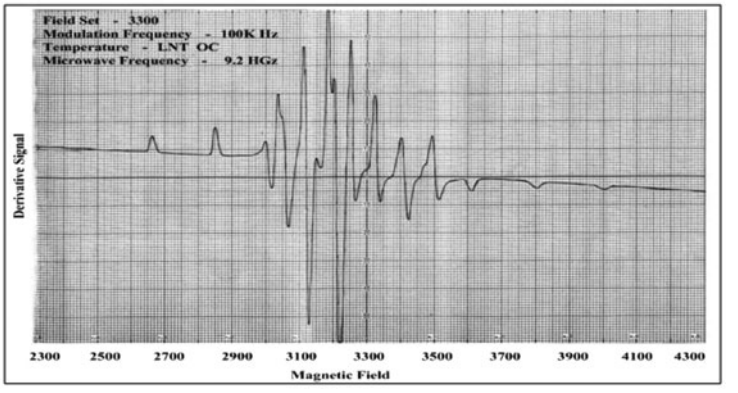

Figure 4. ESR spectrum of [VO(*iso*-vmpph-gls)(H_2O)].

Table 5. ESR spectral parameters of the complexes.

Compound	$A_\perp$	$A_\parallel$	A_{av}	$g_\perp$	$g_\parallel$	g_{av}
[VO(bmpph-gls)(H_2O)]	44	190	92.67	2.021	1.970	2.004
[VO(*iso*-vmpph-gls)(H_2O)]	50	190	96.67	2.021	1.972	2.005

Table 6. Electronic spectral data of some complexes.

Complexes	λ_{max} (nm) (ε, L M^{-1} cm^{-1})	Peak assignment
[VO(bmpph-gls)(H_2O]	295(3441)	Charge transfer transition
	336(2543)	Charge transfer transition
	442(500)	$b_2 \rightarrow a_1^*$
	625(50)	$b_2 \rightarrow b_1^*$
[VO(*iso*-vmpph-gls)(H_2O]	295(3259)	Charge transfer transition
	306(3240)	Charge transfer transition
	317(3180)	Charge transfer transition
	443(375)	$b_2 \rightarrow a_1^*$
	580(50)	$b_2 \rightarrow b_1^*$
[VO(vmpph-gls)(H_2O)]	289(3139)	Charge transfer transition
	444(424)	$b_2 \rightarrow a_1^*$
	575(40)	$b_2 \rightarrow b_1^*$

the range 1.68–1.71 BM, as expected for a simple $S = 1/2$ paramagnet with a d_{xy} based ground state [67]. These data suggest that the complexes under this investigation are mononuclear and paramagnetic [68].

5.4. *ESR spectral studies*

The X-band EPR spectra of **1** and **3** were recorded in frozen DMF solution without DPPH at LNT. The spectra were recorded using the microwave frequencies 9.2 and 9.18 GHz, respectively (figures 3 and 4). Each spectrum shows an eight-line pattern, characteristic of an unpaired electron coupled with a vanadium nuclear spin ($I = 7/2$) revealing the hyperfine

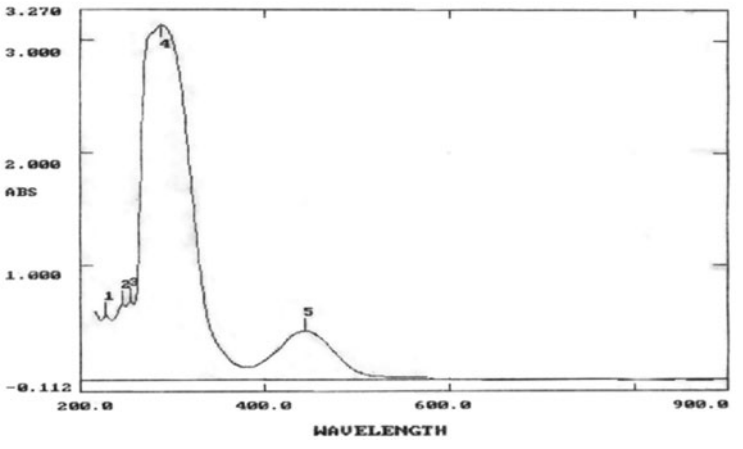

Figure 5. Electronic spectrum of [VO(vmpph-gls)(H_2O)].

splitting of the nucleus. This means that the unpaired electron is in the vicinity of $I = 7/2$ of vanadium. The calculations of $g_\perp$, $g_\parallel$, and g_{av} values in each of the complexes are given in table 5.

The $g_{||}$ and $g_\perp$ values in the two complexes mentioned in table 5 deviate from the free ion value 2.0036, which suggests that the resulting complexes are covalent [67]. From the values obtained for $g_\perp$, $g_{||}$, and g_{av}, it is evident that the unpaired electron is present in d_{xy} orbital [69]. Moreover, the features like spin Hamiltonian parameters $A_\perp$ and $A_{||}$ values are obtained from the spectra of these compounds. The respective values indicate monomeric oxovanadium(IV) complexes [70] and hence the possibility of an octahedron is eradicated. This clearly depicts that the compounds are trigonal pyramidal or square pyramidal.

5.5. *Electronic spectral studies*

The electronic spectra of **1**, **3**, and **7** were recorded in 10^{-3} M DMF solution. λ_{max} of electronic spectral peaks, their molar extinction coefficients, and tentative assignments are given in table 6. Compound **1** displayed four spectral peaks at 295, 336, 442, and 625 nm.

Table 7. Selected geometrical parameters of [VO(ampph-gls)(H_2O)].

Bond connectivity	Length	Bond connectivity	Angle	Bond connectivity	Dihedral angle
V(14)–O(16)	2.218	N(11)–V(14)–O(15)	114.092	V(14)–N(11)–C(13)–C(27)	−9.305
V(14)–O(15)	1.602	N(11)–V(14)–H(10)	81.750	V(14)–N(11)–C(13)–C(30)	167.566
V(14)–O(17)	2.045	N(11)–V(14)–O(17)	121.437	C(3)–N(11)–V(14)–O(10)	−14.497
V(14)–O(10)	1.859	N(11)–V(14)–O(16)	99.024	C(3)–N(11)–V(14)–O(15)	−119.464
V(14)–N–(11)	2.037	O(15)–V(14)–O(17)	124.458	C(3)–N(11)–V(14)–O(16)	139.555
C(13)–N(11)	2.6143	O(16)–V(14)–O(10)	154.340	C(3)–N(11)–V(14)–O(17)	61.758
		O(16)–V(14)–O(17)	74.934	C(3)–N(11)–V(14)–H(45)	−158.787
		O(10)–V(14)–O(17)	82.774	C(13)–N(11)–V(14)–O(10)	158.822
		O(15)–V(14)–O(16)	96.183	C(13)–N(11)–V(14)–O(15)	53.854
				C(13)–N(11)–V(14)–O(16)	−47.125
				C(13)–N(11)–V(14)–O(17)	−124.922
				C(13)–N(11)–V(14)–H(45)	14.532

The first two peaks of relatively higher molar extinction coefficients are due to charge transfer transitions, while the remaining two peaks of lower extinction coefficients may be due to $b_2 \rightarrow a_1^*$ and $b_2 \rightarrow b_1^*$ transitions, respectively. Compound **3** displayed three charge transfer transitions and two d–d transitions, while compound **7** displayed one charge transfer transition and two d–d transitions (figure 5). These transitions are in agreement with the spectral data reported elsewhere and suggest square pyramidal geometry [71] for these complexes.

5.6. *Thermal analysis*

TG analysis of one representative compound [VO(bmpph-gls)(H_2O)] (MW = 521.94) was performed on a PerkinElmer (Pyris Diamond) Thermoanalyzer at Institute Instrumentation Center, IIT, Roorkee (Supplementary material). The TG curve was recorded from room temperature up to 800 °C at a heating rate of 10 ° min^{-1} in nitrogen. The complex shows a weight loss at 135 °C ,which corresponds to the loss of one coordinated water [(observed) 3.75/(calculated) 3.45%]. The TG curve shows another weight loss at 396 °C, which corresponds to the loss of 3-OH groups present in the glucosamine moiety of the ligand

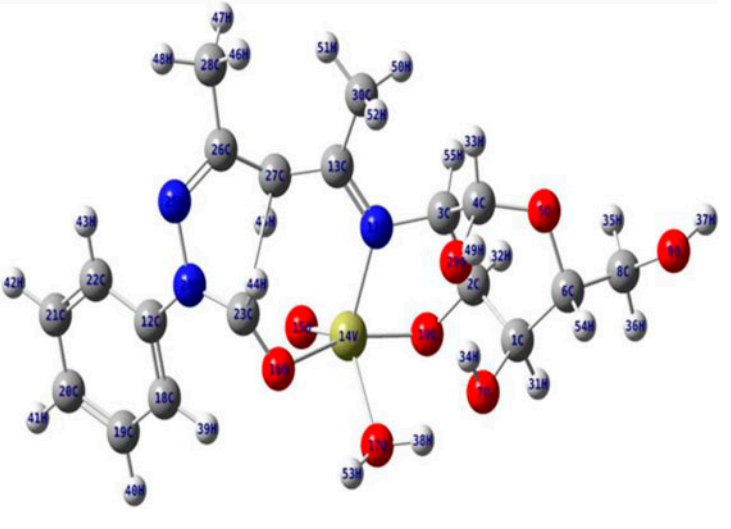

Figure 6. Optimized structure of [VO(ampph-gls)(H_2O)].

[(observed) 8.7/(calculated) 10.1%]. The TG curve shows a weight loss at 455 °C, corresponding to the complete removal of glucosamine unit from the complex [(observed) 26.64/(calculated) 27.4%]. The final residue attaining a constant weight [(observed) 51.26/(calculated) 40.73%] over 660 °C roughly corresponds to V_2O_5. TGA based thermodynamic and kinetic evaluation has been given in Supplementary material.

5.7. *Geometrical parameters*

The various bond lengths, bond angles, and dihedral angles generated from the optimized structure of one of the representative complexes, [VO(ampph-gls)(H_2O)] using Gaussian 09 software are given in table 7. The computed bond lengths, such as V=O(oxo) (15), V–O (enolic) (10), V–N (11), and V–O(water) (17), in the present complex are 1.602, 1.859, 2.037, and 2.045 Å, respectively. These results are comparable to the data reported elsewhere [72, 73]. The significant computed bond angles in the complex, such as N(11)–V(14)–O(10), (81.75°), O(16)–V(14)–O(17), (74.93°), O(10)–V(14)–O(17), (82.77°), O(15)–V(14)–O(17), (124.458°), O(15)–V(14)–O(10), (106.972°), O(15)–V(14)–N(11), (114.092°), and O(15)–V(14)–O(16), (96.18°), suggest the square pyramidal structure of the complexes. The optimized structure of [VO(ampph-gls)(H_2O)] is shown in figure 6.

Quantitatively, the angular structural parameter τ proposed by Addison *et al.* [74] may also be used to distinguish between TB and SP structures, evaluated as

$$\tau = \frac{\beta - \alpha}{60}$$

where α and β are bond angles, O_{10}–V_{14}–O_{17} and N_{11}–V_{14}–O_{16}, respectively, taking $\beta \geq \alpha$. Here, $\beta = 99.02$ and $\alpha = 82.77$.

For purely SP polyhedra, τ is 0 and for a perfect TB polyhedron τ is 1. Corman *et al.* applied this parameter and described vanadyl complexes with $0 < \tau < 0.5$ as distorted SP, while complexes with $0.5 < \tau < 1$ were considered as distorted TB [75]. Computationally, it is found that $\tau = 0.271$ for [VO(ampph-gls)(H_2O)], confirming SP geometry.

5.8. *Frontier molecular orbitals analysis*

The HOMO is the orbital that primarily acts as an electron donor and the LUMO is the orbital that largely acts as the electron acceptor, and the gap between HOMO and LUMO characterizes the molecular stability [76, 77]. Four important molecular orbitals, second highest [HOMO-1], and highest occupied MO's [HOMO], the lowest [LUMO], and second lowest unoccupied MO's [LUMO+1], have been worked out for H_2ampph-gls as −0.23730, −0.16934, −0.06547, and −0.01903 a.u., respectively, and the energy gaps (ΔE) between [HOMO–LUMO] and [HOMO-1–LUMO+1], for H_2ampph-gls are −0.10387 and −0.21827 a.u., respectively. Similarly, [HOMO-1], [HOMO], [LUMO], and [LUMO+1] are worked

Table 8. Absolute electronegativity (χ_{abs}), absolute hardness (η), electrophilicity index (ω), and global softness (S) of [VO(ampph-gls)(H_2O)].

Compounds	χ_{abs}	η	ω	S
H_2ampph-gls	−0.11737	−0.05193	−129.98	−19.25
[VO(ampph-gls)(H_2O)]	−0.12809	−0.06214	−384.91	−16.09

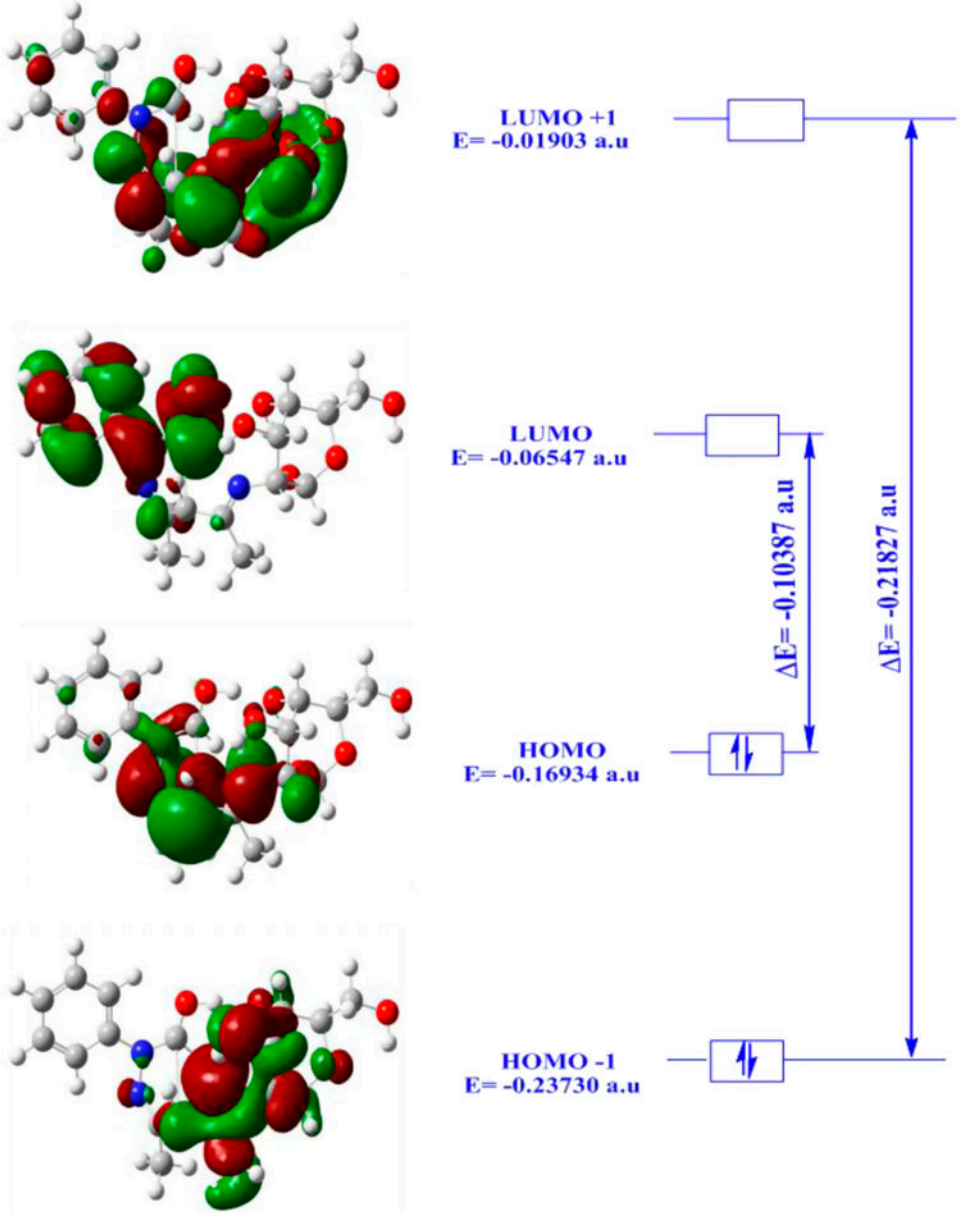

Figure 7. HOMO–LUMO structure with energy-level diagram of [H_2ampph-gls].

out for [VO(ampph)(gls)(H_2O), and the observed energies in the same order are −0.21329, −0.19023, −0.06595, and −0.04572 a.u., respectively, while the energy gaps between [HOMO–LUMO] and [HOMO-1–LUMO+1] are −0.12428 and −0.16757 a.u., respectively. The presence of one unpaired electron in the HOMO in the complex justifies that it is paramagnetic with a singly occupied molecular orbital (SOMO).

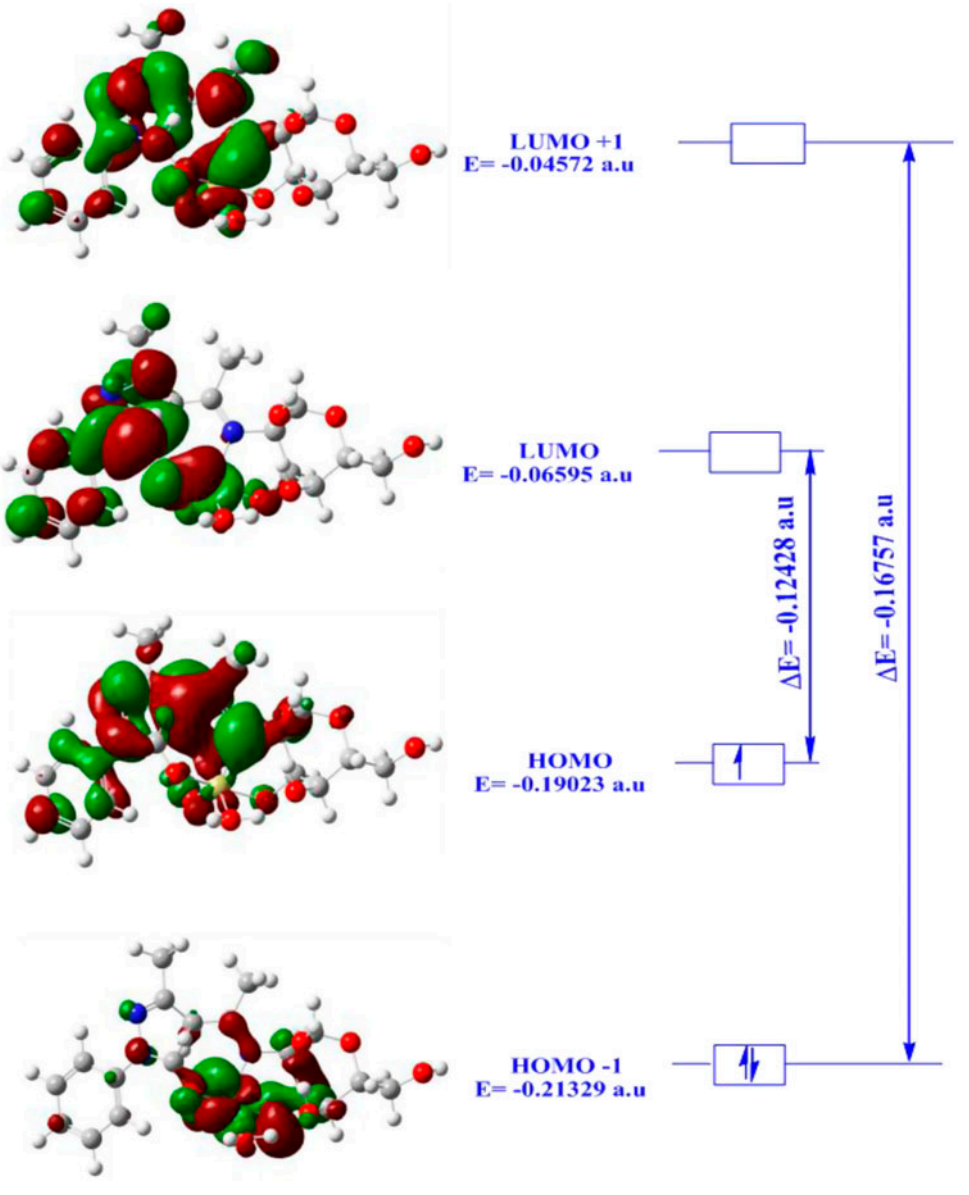

Figure 8. HOMO–LUMO structure with energy-level diagram of [VO(ampph-gls)(H_2O)].

The energy of the frontier orbitals for molecules in terms of ionization energy (IE) and electron affinity (IA) of the H_2ampph-gls and its complex from Koopmans's theorem [78] are:

$$-E_{HOMO} = IE \quad (1)$$

$$-E_{LUMO} = EA \quad (2)$$

The absolute electronegativity (χ_{abs}) and absolute hardness (η) are related to IA and EA [79] as given below:

$$\chi_{abs} = (IE + IA)/2 = (E_{HOMO} + E_{LUMO})/2 \tag{3}$$

$$\eta = (IE - IA)/2 = (E_{HOMO} - E_{LUMO})/2 \tag{4}$$

Hard molecules have a large HOMO–LUMO gap and soft molecules have a small HOMO–LUMO gap [80]. The absolute electronegativity (χ_{abs}) and absolute hardness (η) of dehydroacetic acid and its complex calculated using equations (3) and (4) are provided in table 8. There is a very short gap between HOMO and LUMO in its complex as compared with ligands. The HOMO–LUMO structures with energy-level diagram of H_2ampph-gls and its complex are shown in figures 7 and 8, respectively.

Another important property related to the dipole moment and hardness is electrophilicity index (ω) and global softness (S), shown in equation below. The values of ω and S are given in table 8.

$$\omega = \mu^2/2\eta \tag{5}$$

$$S = 1/\eta \tag{6}$$

5.9. *Hyperpolarizability calculations*

DFT has been used to calculate the dipole moment (μ), mean polarizability (α), and the total first static hyperpolarizability (β_0) [81, 82] for [VO(ampph-gls)(H_2O)] in terms of x, y, and z components from the following equations.

$$\mu = (\mu_x^2 + \mu_y^2 + \mu_z^2)^{1/2} \tag{7}$$

$$\alpha = 1/3(\alpha_{xx} + \alpha_{yy} + \alpha_{zz}) \tag{8}$$

$$\Delta\alpha = \left[\frac{(\alpha_{XX} - \alpha_{YY})^2 + (\alpha_{YY} - \alpha_{ZZ})^2 + (\alpha_{ZZ} - \alpha_{XX})^2}{2}\right]^{1/2} \tag{9}$$

$$\beta_0 = (\beta_x^2 + \beta_y^2 + \beta_z^2)^{1/2} \tag{10}$$

and

$$\beta_x = \beta_{xxx} + \beta_{xyy} + \beta_{xzz}$$

$$\beta_y = \beta_{yyy} + \beta_{xxy} + \beta_{yzz}$$

Table 9. Calculated all (μ, β, and α) components, (μ, α) total, and (β_0, $\Delta\alpha$) of [VO(ampph-gls)(H_2O)].

Dipole moment (μ)		Hyperpolarizability (β)	
μ_x	4.3940	β_{xxx}	120.6982
μ_y	4.3691	β_{yyy}	11.8355
μ_z	2.3093	β_{zzz}	46.3724
μ_{total}	6.6128	β_{xxx}	10.0508
Polarizability (α)		β_{xxy}	−64.0494
α_{xx}	−170.7632	β_{xxz}	−152.4655
α_{yy}	−175.2481	β_{xzz}	85.0393
α_{zz}	−182.9920	β_{yzz}	4.0446
α_{xy}	2.5752	β_{yyz}	19.0255
α_{xz}	−8.7253	β_{xyz}	22.7244
α_{yz}	−5.7772	β_0	237.625
α total	−176.3344		
$\Delta\alpha$	10.751		

Note: α_{xx}, α_{yy}, and α_{zz} are tensor components of polarizability: β_{iiz}, β_{izi}, and β_{zii} (i from x to z) are tensor components of hyperpolarizability: μ_x, μ_y, and μ_z are the components of the dipole moment. α is the mean polarizability, $\Delta\alpha$ is the anisotropy of polarizability, and β_0 is the mean first hyperpolarizability.

Table 10. Data of Mulliken and NBO atomic charges of [VO(ampph-gls)(H_2O)].

Atoms	NBO atomic charges	Mulliken atomic charges	Atoms	NBO atomic charges	Mulliken atomic charges
1 C	−0.083	0.076	29 O	−0.524	−0.822
2 C	0.004	0.109	30 C	−0.786	−0.679
3 C	−0.095	−0.095	31 H	0.238	0.242
4 C	−0.071	0.441	32 H	0.192	0.213
5 O	−0.298	−0.648	33 H	0.243	0.210
6 C	0.008	0.072	34 H	0.408	0.517
7 O	−0.578	−0.828	35 H	0.199	0.196
8 C	−0.319	−0.056	36 H	0.188	0.192
9 O	−0.478	−0.788	37 H	0.352	0.487
10 O	−0.506	−0.669	38 H	0.484	0.555
11 N	−0.481	−0.636	39 H	0.275	0.248
12 C	0.372	0.150	40 H	0.220	0.222
13 C	0.444	0.322	41 H	0.221	0.219
14 V	0.865	0.884	42 H	0.219	0.220
15 O	−0.373	−0.391	43 H	0.272	0.244
16 O	−0.405	−0.685	44 H	0.240	0.191
17 O	−0.770	−0.903	45 H	0.302	0.240
18 C	−0.268	−0.217	46 H	0.216	0.231
19 C	−0.213	−0.198	47 H	0.226	0.235
20 C	−0.237	−0.218	48 H	0.245	0.250
21 C	−0.198	−0.206	49 H	0.385	0.508
22 C	−0.346	−0.224	50 H	0.221	0.226
23 C	−0.030	0.567	51 H	0.252	0.232
24 N	−0.179	−0.292	52 H	0.221	0.227
25 N	−0.129	−0.386	53 H	0.418	0.532
26 C	0.144	0.319	54 H	0.249	0.240
27 C	−0.449	−0.428	55 H	0.222	0.229
28 C	−0.736	−0.668			

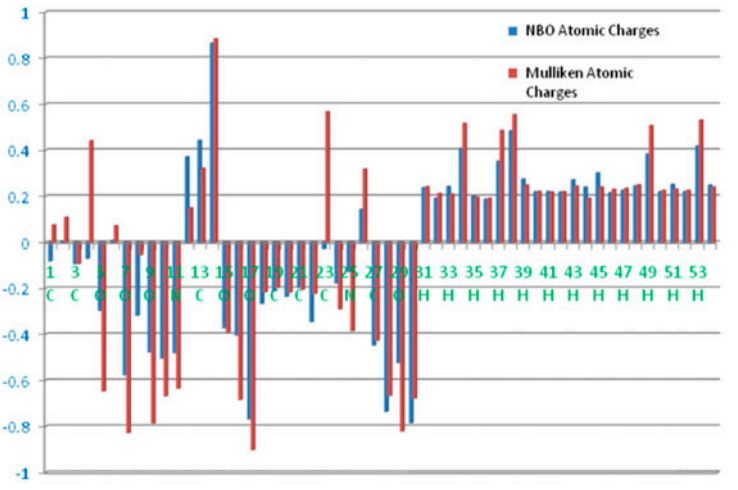

Figure 9. Graphical representation of Mulliken and NBO atomic charges of [VO(ampph-gls)(H_2O)].

$$\beta_z = \beta_{zzz} + \beta_{xxz} + \beta_{yyz}$$

(or)

$$\beta_0 = [(\beta_{xxx} + \beta_{xyy} + \beta_{xzz})^2 + (\beta_{yyy} + \beta_{yzz} + \beta_{yxx})^2 + (\beta_{zzz} + \beta_{zxx} + \beta_{zyy})^2]^{1/2} \quad (11)$$

The calculated electric dipole moment μ (Debye), isotropic polarizability, α (in a.u.), anisotropy of the polarizability, $\Delta\alpha$ (in a.u.), and all hyperpolarizability (β) components (in a.u.) values are given in table 9.

5.10. *Atomic net charges*

The natural atomic charges of [VO(ampph)(acac)(H_2O)] obtained by NBO and Mulliken population analysis [83] with B3LYP/LANL2DZ basis set are compared in table 10. The comparison between Mulliken net charges and the atomic natural ones is not an easy task, since the theoretical background of the two methods is very different. Looking at the results there are surprising differences between the Mulliken and the NBO charges. The data indicate that C_2, C_6, C_{12}, C_{13}, C_{18}, C_{19}, C_{20}, C_{21}, C_{22}, C_{26}, C_{27}, C_{28}, C_{30}, and all hydrogens bear positive charge in both NBO and Mulliken analyses. V_{14} also bears positive charge in NBO analysis as well as in Mulliken analysis. The remaining atoms: C_3, C_8, C_{17}, N_{11}, N_{24}, and N_{25}, and all oxygens, O_5, O_7, O_9, O_{10}, O_{16}, O_{17} and O_{29}, bear negative charges in both analyses. These are clearly shown in the graphical representation of NBO and Mulliken charges given in figure 9. The color range in the scale of positive and negative charges and graphical representation for (a) Mulliken atomic charges and (b) NBO atomic charges of the complex are shown in figure 10.

The definition of Mulliken charges is based on population analysis. The Mulliken population analysis provides a partitioning of either the total charge density or an orbital density. The number of electrons in the molecule (N) is the integral of the charge density over space. N is partitioned for all atoms, considering also the overlap population. According to

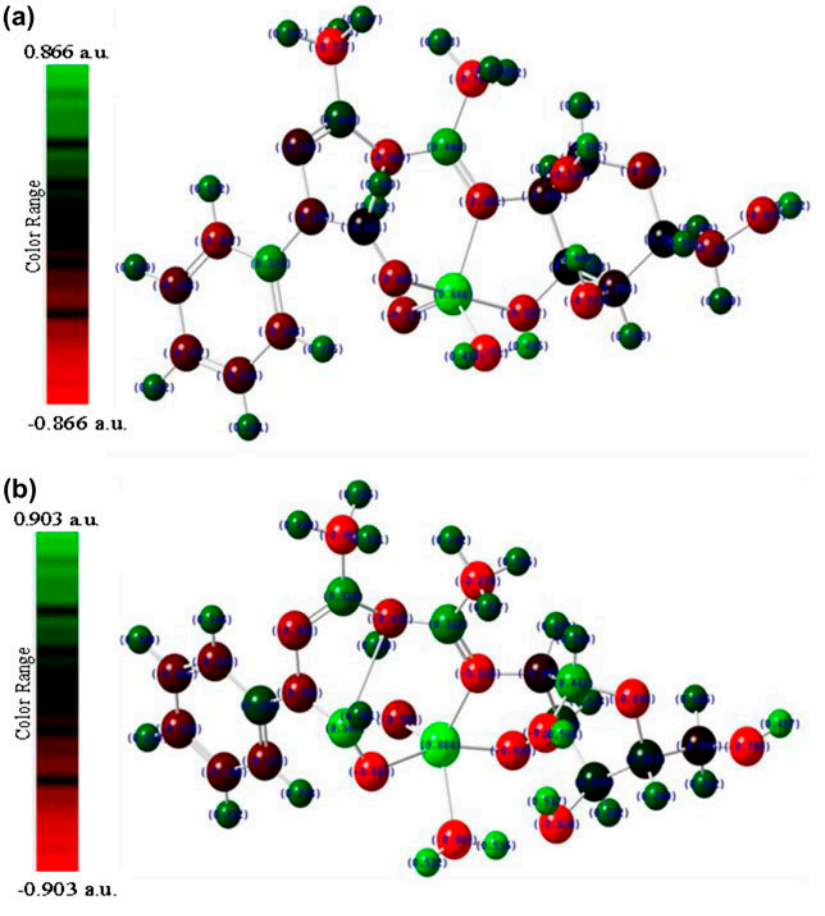

Figure 10. Structure with color range of (a) Mulliken atomic charges and (b) NBO atomic charges of [VO(ampph-gls)(H_2O)].

the theory, the overlap population of atoms A and B is divided between the two atoms in half-to-half ratio. This is one weak point of the theory. The other weak point is its strong dependence on the basis set applied. The atomic net charge is the difference between the calculated number of electrons belonging to the atom in the complex and the number of electrons of the isolated atom.

The natural atomic charge is based on the theory of the natural population analysis. The analysis is carried out with NBO. They are linear combinations of the natural atomic orbitals. The derivation of a valence shell atomic orbital (NAO) involves diagonalization of the localized block of the full density matrix of a given molecule associated with basic functions on that atom. A distinguishing feature of NAOs is that they meet the simultaneous requirement of orthonormality and maximum occupancy. In a polyatomic molecule, the NAOs mostly retain one-center character, and thus they are optimal for describing the molecular electron density around each atomic center. Natural bond orbitals are linear combinations of the NAOs of two bonded atoms. The natural population analysis satisfies Pauli's exclusion principle, and solves the basis set dependence problem of the Mulliken population analysis [84].

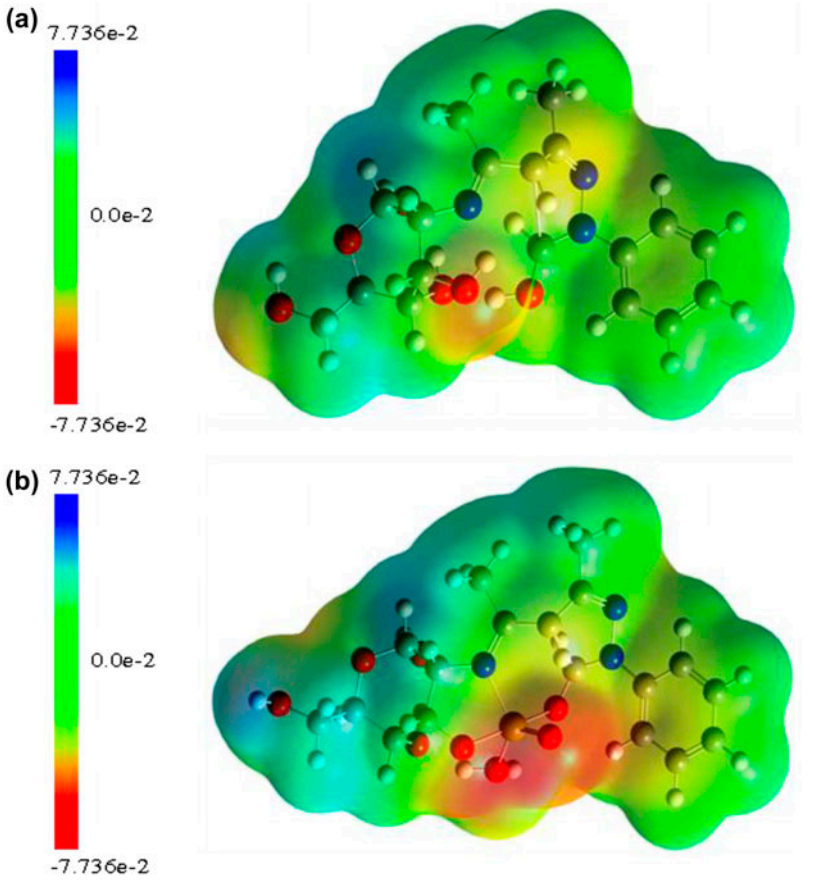

Figure 11. Molecular electrostatic potential MESP (a) [H_2ampph-gls] and (b) [VO(ampph-gls)(H_2O)] with color range along with scale.

5.11. *Molecular surface electrostatic potential of ligand and its complex*

The molecular surface electrostatic potential (MSEP) surface diagram is used to understand the reactive behavior of a molecule, in that negative regions can be regarded as nucleophilic centers, whereas the positive regions are potential electrophilic sites. The molecular electrostatic potential surface [80] (figure 11) displays molecular shape, size, and electrostatic potential values of H_2appmh-gls and its vanadium complex. The MSEP map of H_2appmh-gls shows that the carbonyl and hydroxyl oxygens represent the most negative potential region, while in the case of the complex, the coordination environment of four oxygens and vanadium (central atom) is the region of most negative potential. The hydrogen and nitrogens in H_2appmh-gls bear the region of maximum positive charge. The two hydrogens attached to oxygen of the coordinated water are mostly electropositive. The predominance of green region in the MSEP surfaces corresponds to a potential halfway between the two extremes, red and dark blue color.

6. Conclusion

From the overall structural elucidation of the newly synthesized class of amino sugar Schiff bases, these compounds behave as dibasic tridentate ligands. The satisfactory analytical data coupled with the studies presented suggest that the oxovanadium(IV) complexes are $[VO(L)(H_2O)]$, where H_2L = N-(4′-benzoylidene-3′-methyl-1′-phenyl-2′-pyrazolin-5′-one)-glucosamine, N-(4′-butyrylidene-3′-methyl-1′-phenyl-2′-pyrazolin-5′-one)-glucosamine, N-(3′-methyl-1′-phenyl-4′-*iso*-valerylidene-2′-pyrazolin-5′-one)-glucosamine, N-(3′-methyl-1′-phenyl-4′-propionylidene-2′-pyrazolin-5′-one)-glucosamine, N-(4′-*iso*-butyry lidene-3′-methyl-1′-phenyl-2′-pyrazolin-5′-one)-glucosamine, N-(4′-acetylidene-3′-methyl-1′-phenyl-2′-pyrazolin-5′-one)-glucosamine, and N-(3′-methyl-1′-phenyl-4′-valerylidene-2′-pyrazolin-5′-one)-glucosamine. The SOMO (d_{xy}) depicted computationally was found in best fit with the EPR studies, and the DFT optimization together with theoretical/experimental IR studies indicates that these complexes have square pyramidal structures. Thus, a new class of oxovanadium(IV) coordination compounds have been investigated. These complexes might prove useful further in photoluminescence studies and also be practiced as new tools to investigate AD therapy.

Acknowledgements

The authors are thankful to UGC, New Delhi, India for financial support as a Major Research Project [FNo.41-255/2012 (SR)]. Thanks are also due to RSIC, IIT, Chennai, IIT, Mumbai, and IIT Roorkee for various analyses. We also acknowledge the Department of Chemistry and Pharmacy, Rani Durgavati University, Jabalpur, for providing laboratory facilities.

Supplemental data

Supplemental data for this article can be accessed here. [http://dx.doi.org/10.1080/00958972.2014.959508]

References

[1] M.J. Adam, L.D. Hall. *J. Chem. Soc., Chem. Commun.*, **18**, 234 (1979).
[2] M.J. Adam, L.D. Hall. *Can. J. Chem.*, **60**, 2229 (1982).
[3] J.C. Irvine, J.C. Earl. *J. Chem. Soc., Trans.*, **121**, 2376 (1922).
[4] M. Bergmann, L. Zervas. *Ber. Chem. Ges.*, **64**, 975 (1931).
[5] A. Neuberger. *Biochem. J.*, **32**, 1435 (1938).
[6] Z.E. Jolles, W.T.J. Morgan. *Biochem. J.*, **34**, 1183 (1940).
[7] C. Feng, Z. Le, X. Zhang, X. Zhu, Z. Wu, Z. Yan. *J. Cent. China Normal Univ.*, **28**, 499 (1994).
[8] T. Storr, L.E. Scott, M.L. Bowen, D.E. Green, K.H. Thompson, H.J. Schugarand, C. Orvig. *Dalton Trans.*, **16**, 3034 (2009); Chemistry World, a RSC Magazine, p. 30, June 2009.
[9] K.H. Thompson, J.H. McNeill, C. Orvig. *Chem. Rev.*, **99**, 2561 (1999).
[10] D.C. Crans, S.S. Amin, A.D. Keramaidas. In *Vanadium in the Environment. Part I: Chemistry and Biochemistry*, J.O. Nriagu (Ed.), Chap. 4, pp. 73–95, Wiley, New York (1998).
[11] G.R. Willsky. In: *Vanadium in Biological Systems*, N.D. Chasteen (Ed.), Chap. 1, pp. 1–24, Kluwer Academic, Dordrecht (1990).
[12] D. Rehder. *J. Inorg. Biochem.*, **80**, 133 (2000).
[13] M.R. Maurya, A. Kumar, J. Costa Pessoa. *Coord. Chem. Rev.*, **255**, 2315 (2011).

[14] D. Gambino. *Coord. Chem. Rev.*, **255**, 2193 (2011).
[15] H. Zhang, Y. Yi, D. Feng, Y. Wang, S. Qin. *Evid. Based Complement. Alternat. Med.*, **8**, 1 (2011).
[16] J.C. Dabrowiak. *Metals in Medicine*, p. 221, Wiley, Chichester (2009).
[17] K.H. Thompson, J. Lichter, C. LeBel, M.C. Scaife, J.H. McNeill, C. Orvig. *J. Inorg. Biochem.*, **103**, 554 (2009).
[18] D.C. Crans, J.J. Smee, E. Gaidamauskas, L.Q. Yang. *Chem. Rev.*, **104**, 849 (2004).
[19] K.G. Peters, M.G. Davis, B.W. Howard, M. Pokross, V. Rastogi, C. Diven, K.D. Greis, E. Eby-Wilkens, M. Maier, A. Evdokimov, S. Soper, F. Genbauffe. *J. Inorg. Biochem.*, **96**, 321 (2003).
[20] B. Jing, J. Dong, J. Li, T. Xu, L. Li. *J. Coord. Chem.*, **66**, 520 (2013).
[21] R. Takjoo, J.T. Mague, A. Akbari, S.Y. Ebrahimipour. *J. Coord. Chem.*, **66**, 2852 (2013).
[22] M. Amini, A. Arab, R. Soleyman, A. Ellern, L. Keith Wood. *J. Coord. Chem.*, **66**, 3770 (2013).
[23] Z.H. Chohan, S.H. Sumrra, M.H. Youssoufi, T.B. Hadda. *J. Coord. Chem.*, **63**, 3981 (2010).
[24] K. Nagaraju, A. Sarkar, S. Pal. *J. Coord. Chem.*, **66**, 77 (2013).
[25] E.J. Baran. *J. Coord. Chem.*, **54**, 215 (2001).
[26] A. Abbas, H. Nazir, M.M. Naseer, M. Bolte, S. Hussain, N. Hafeez, A. Hasan. *Spectrochim. Acta, Part A*, **120**, 176 (2014).
[27] M. Karuppasamy, M. Mahapatra, S. Yabanoglu, G. Ucar, B.N. Sinha, A. Basu, N. Mishra, A. Sharon, U. Kulandaivelu, V. Jayaprakash. *Bioorg. Chem.*, **18**, 1875 (2010).
[28] R.H. Wiley, P. Wiley. *The Chemistry of Heterocyclic Compounds, Pyrazolones Pyrazolidines, and Derivatives*, Interscience, New York (1964).
[29] L.S. Goodman, A. Gilman, A. Gilman. *The Pharmacological Basis of Therapeutics*, p. 4, Macmillan, London (1970).
[30] E. McDonald, K. Jones, P.A. Brough, M.J. Drysdale, P. Workman. *Curr. Top. Med. Chem.*, **6**, 1193 (2006).
[31] J. Elguero. In: *Comprehensive Heterocyclic Chemistry*, A.R. Katritzky, C.W. Rees, E.F.V. Scriven (Eds), Vol. 5, Pergamon, Oxford (1996); (b) J. Elguero, P. Goya, N. Jagerovic, A.M.S. Silva. *Targets Heterocycl. Syst.*, **6**, 52 (2002).
[32] B. Gyurcsik, L. Nagy. *Coord. Chem. Rev.*, **203**, 81 (2000).
[33] S.B. Etcheverry, P.A.M. Williams, E.J. Baran. *J. Inorg. Biochem.*, **63**, 285 (1996).
[34] Y. Allegretti, E.G. Ferrer, A.C. González Baró, P.A.M. Williams. *Polyhedron*, **19**, 2613 (2000).
[35] R. Codd, T.W. Hambley, P.A. Lay. *Inorg. Chem.*, **34**, 877 (1995).
[36] P.A.M. Williams, S.B. Etcheverry, E.J. Baran. *J. Inorg. Biochem.*, **65**, 133 (1997).
[37] J. Ruiz, C. Floriani, A. Chiesi-Villa, C. Guastini. *J. Chem. Soc., Dalton Trans.*, 2467 (1991).
[38] U. Piarulli, D.N. Williams, C. Floriani, G. Gervasio, D. Viterbo. *J. Chem. Soc., Chem. Commun.*, 1409 (1994). doi:10.1039/c39940001409
[39] B. Zhang, S. Zhang, K. Wang. *J. Chem. Soc., Dalton Trans.*, 3257 (1996).
[40] T.E. McAlindon, M.P. LaValley, J.P. Gulin, D.T. Felson. *J. Am. Med. Assoc.*, **283**, 1469 (2000).
[41] T.E. Towheed, T.P. Anastassiades. *J. Am. Med. Assoc.*, **283**, 1483 (2000).
[42] L. Gerhardsson, K. Blennow, T. Lundh, E. Londos, L. Minthon. *Dement. Geriatr. Cogn. Disord.*, **28**, 88 (2009).
[43] L. Gerhardsson, T. Lundh, E. Londos, L. Minthon. *J. Neural Trans.*, **118**, 957 (2011).
[44] A.M. Ektessabi, S. Fujisawa, K. Takada, K. Yoshida, H. Murayama, R.W. Shin. *Int. J. PIXE.*, **9**, 297 (1999).
[45] H. Guo, J. Lu, Z. Ruan, Y. Zhang, Y. Liu, L. Zang, J. Jiang, J. Huang. *J. Coord. Chem.*, **65**, 191 (2012).
[46] A.A. Soliman. *J. Therm. Anal. Calorim.*, **31**, 63 (2001).
[47] G.G. Mohamed, Z.H. Abdel-Wahab. *J. Therm. Anal. Calorim.*, **59**, 73 (2003).
[48] H.A. El-Boraey. *J. Therm. Anal. Calorim.*, **81**, 339 (2005).
[49] S.H. Patel, P.B. Pansuriya, M.R. Chhasatia, H.M. Parekh, M.N. Patel. *J. Therm. Anal. Calorim.*, **91**, 413 (2008).
[50] E. Garribba, E. Lodyga-Chruscinska, G. Micera. *Inorg. Chem.*, **50**, 883 (2011).
[51] G.S. Rodrigues, I. Da Silva Cunha, G.G. Silva, A.L.O. De Noronha, H.A. De Abreu, H.A. Duarte. *Inc. Int. J. Quantum Chem.*, **111**, 1395 (2011).
[52] G. Micera, E. Garribba. *J. Comp. Chem.*, **32**, 2822 (2011).
[53] M.R. Maurya, M. Bisht, A. Kumar, M.L. Kuznetsov, F. Avecilla, J.C. Pessoa. *Dalton Trans.*, **40**, 6968 (2011).
[54] K.T. Scior, H.G. Mack, J.A.G. Garcia, W. Koch. *Drug Des. Dev. Ther.*, **2**, 221 (2008).
[55] R. Jacob, G. Fischer. *J. Mol. Struct.*, **613**, 175 (2002).
[56] J. Jayabharathi, V. Thanikachalam, M.. Venkatesh Perumal. *Spectrochim. Acta, Part A*, **95**, 614 (2012).
[57] N.H. Furman. *Standard Methods of Chemical Analysis*, 6th Edn, Vol. 1, p. 1211, Van Nostrand Company, Inc., NJ (1962).
[58] M.J. Frisch, G.W. Trucks, H.B. Schlegel, G.E. Scuseria, M.A. Robb, J.R. Cheeseman, G. Scalmani, V. Barone, B. Mennucci, G.A. Petersson, H. Nakatsuji, M. Caricato, X. Li, H.P. Hratchian, A.F. Izmaylov, J. Bloino, G. Zheng, J.L. Sonnenberg, M. Hada, M. Ehara, K. Toyota, R. Fukuda, J. Hasegawa, M. Ishida, T. Nakajima, Y. Honda, O. Kitao, H. Nakai, T. Vreven, J.A. Montgomery Jr., J.E. Peralta, F. Ogliaro, M. Bearpark, J.J. Heyd, E. Brothers, K.N. Kudin, V.N. Staroverov, T. Keith, R. Kobayashi, J. Normand, K. Raghavachari, A. Rendell, J.C. Burant, S.S. Iyengar, J. Tomasi, M. Cossi, N. Rega, J.M. Millam, M. Klene, J.E. Knox,

J.B. Cross, V. Bakken, C. Adamo, J. Jaramillo, R. Gomperts, R.E. Stratmann, O. Yazyev, A.J. Austin, R. Cammi, C. Pomelli, J.W. Ochterski, R.L. Martin, K. Morokuma, V.G. Zakrzewski, G.A. Voth, P. Salvador, J.J. Dannenberg, S. Dapprich, A.D. Daniels, O. Farkas, J.B. Foresman, J.V. Ortiz, J. Cioslowski, D.J. Fox. *GAUSSIAN 09 (Revision C.01)*, Gaussian, Inc., Wallingford, CT (2010).
[59] GaussView 5.0. Gaussian Inc., Garnegieoffice Park, Pittsburgh, PA, USA (2008).
[60] S. Bayari, S. Saglan, H.F. Ustundag. *THEOCHEM.*, **726**, 226 (2005).
[61] R.C. Maurya, P. Patel, S. Rajput. *Synth. React. Inorg.-Met. Org. Chem.*, **33**, 801 (2003).
[62] R.C. Maurya, H. Singh, A. Pandey, T. Singh. *Indian J. Chem.*, **40(A)**, 1053 (2001).
[63] L.V. Boas, J.C. Pessoa, G. Wilkinson, R.D. Gillard, J.A. McCleverty (Eds.). *Comprehensive Coordination Chemistry*, 1st Edn, p. 540, Pergamon Press, Oxford (1987).
[64] T.A. Alsalim, J.S. Hadi, O.N. Ali, H.S. Abbo, S.J.J. Titinchi. *Chem. Cent. J.*, **7**, 3 (2013). doi:10.1186/1752-153X-7-3
[65] J. Costa Pessoa, I. Tomaz, R.T. Henriques. *Inorg. Chim. Acta*, **356**, 121 (2003).
[66] W.J. Geary. *Coord. Chem. Rev.*, **7**, 81 (1971).
[67] S.K. Dutta, R.T.T. Edward, M. Chaudhury. *Polyhedron*, **16**, 1863 (1997).
[68] R.L. Dutta, A. Syamal. In *Elements of Magnetochemistry*, 2nd Edn, p. 225, Affiliated East-West Press, New Delhi (1993).
[69] G.N. Raja Reddy, S. Kondaiah, K. Nagaraja Setty, R. Mallikarjuna Rao, J. Sree Ramulu. *Orient. J. Chem.*, **28**, 1673 (2012).
[70] R.C. Maurya, H. Singh, A. Pandey. *Synth. React. Inorg.-Met. Org. Chem.*, **32**, 231 (2002).
[71] B.J. Mc Cormick,. *Inorg Chem.*, **1**, 1965 (1968).
[72] N.N. Greenwood, A. Earnshaw. *Chemistry of the Elements*, 1st Edn, Pergamon Press, New York (1984).
[73] R.C. Maurya, S. Rajput. *J. Mol. Struct.*, **687**, 35 (2004).
[74] A.W. Addison, T.N. Rao, J. Reedijk, J. van Rijn, G.C. Verschoor. *J. Chem. Soc., Dalton Trans.*, 1349 (1984).
[75] C.R. Cornman, K.M. Geiser-Bush, S.P. Rowley, P.D. Boyle. *Inorg. Chem.*, **36**, 6401 (1997).
[76] D. Shoba, S. Periandy, M. Karabacak, S. Ramalingam. *Spectrochim. Acta, Part A*, **83**, 540 (2012).
[77] K. Fukui. *Science*, **218**, 747 (1982).
[78] C.J. Brabec, N.S. Sariciftci, J.C. Hummelen. *Adv. Funct. Mater.*, **11**, 15 (2001).
[79] E. Ebenso, T. Arslan, F. Kandemirlı, I. Love, M. Saracoglu, S.A. Umoren. *Int. J. Quantum Chem.*, **110**, 2614 (2010).
[80] R.G. Pearson. *Acc. Chem. Res.*, **26**, 250 (1993).
[81] Y. Sun, X. Chen, L. Sun, X. Guo, W. Lu. *J. Chem. Phys. Lett.*, **381**, 397 (2003).
[82] O. Christiansen, J. Gauss, J.F. Stanton. *J. Chem. Phys. Lett.*, **305**, 147 (1999).
[83] R.S. Mulliken. *J. Chem. Phys.*, **23**, 1833 (1995).
[84] F. Billes, A. Holmgren, H. Mikosch. *Vib. Spectrosc.*, **53**, 296 (2010).